

# Longitudinal tapering in meter-scale gas jets for increased efficiency of laser plasma accelerators

R. Li,<sup>1,2</sup> A. Picksley,<sup>1</sup> C. Benedetti,<sup>1</sup> F. Filippi,<sup>1,3</sup> J. Stackhouse,<sup>1,2</sup> L. Fan-Chiang,<sup>1,4</sup> H. E. Tsai,<sup>1</sup> K. Nakamura,<sup>1</sup> C. B. Schroeder,<sup>1,2,4</sup> J. van Tilborg,<sup>1</sup> E. Esarey,<sup>1</sup> C. G. R. Geddes,<sup>1</sup> and A. J. Gonsalves<sup>1</sup>

<sup>1</sup>*Lawrence Berkeley National Laboratory, 1 Cyclotron Road, Berkeley CA 94720, USA*

<sup>2</sup>*UC Berkeley, Nuclear Engineering, 2505 Hearst Ave, Berkeley, CA 94709, USA*

<sup>3</sup>*ENEA Nuclear Department-C. R. Frascati, Via Enrico Fermi 45, 00044 Frascati, Italy*

<sup>4</sup>*UC Berkeley, Applied Science and Technology, 210 Hearst Ave, Berkeley, CA 94720, USA*

(Dated: 27 November 2024)

Modern laser plasma accelerators (LPAs) often require meter-scale plasma waveguides to propagate a high-intensity drive laser pulse. Tapering the longitudinal gas density profile in meter-scale gas jets could allow for single stage laser plasma acceleration well beyond 10 GeV with current petawatt-class laser systems. Via simulation and interferometry measurements, we show density control by longitudinally adjusting the throat width and jet angle. Density profiles appropriate for tapering were calculated analytically and via particle-in-cell (PIC) simulations, and were matched experimentally. These simulations show that tapering can increase electron beam energy using 19 J laser energy from  $\sim 9$  GeV to  $>12$  GeV in a 30 cm plasma, and the accelerated charge by an order of magnitude.

## I. INTRODUCTION

Laser plasma accelerators (LPAs)<sup>1,2</sup> are a promising technology for building compact accelerators because they can generate electric fields 10-100 GeV/m<sup>2</sup>, which is orders of magnitude higher than conventional accelerators. In an LPA, a high-intensity laser beam's ponderomotive force excites plasma waves, which generate large electric fields inside a plasma. These electric fields are used to accelerate electrons to high energies. LPAs are studied for many applications, including free-electron lasers<sup>3</sup>, high-energy particle colliders<sup>4</sup>, or nuclear detection<sup>5</sup>. Maximizing efficiency, defined as the fraction of laser energy transferred to the electron beam, is crucial for these applications.

Generating 10-GeV-class electron bunches requires a meter-scale accelerator according to scaling laws<sup>2</sup>. Since the Raleigh range for a typical PW-class drive laser is  $\sim 1$  cm, diffraction limits the range where the drive laser is intense enough to drive an LPA. Different techniques have been developed to prevent diffraction, including relativistic self-guiding<sup>6,7</sup> and pre-formed plasma channel waveguides<sup>8-10</sup>, which can be created using the hydrodynamic optical field ionization (HOFI) method<sup>11-14</sup>. Gas jets are a common plasma source for a large variety of laser-plasma interaction experiments, including LPAs in the self-guided or guided regimes. Gas jets based on elongated converging-diverging (de Laval) nozzles have been demonstrated at meter-scale lengths<sup>15,16</sup>. We have recently employed a 30-cm-long gas jet to generate quasimonoenergetic electron beams at 9.2 GeV, with charge extending beyond 10 GeV using HOFI channels and a 21 J, 40 fs drive laser<sup>17</sup>.

In a guided LPA, the energy achievable in a single LPA stage is often limited by dephasing. This occurs when the accelerating electron bunch has a higher velocity than the drive laser, which travels at the group velocity of light in a plasma  $v_g < c$ . Eventually, the electron bunch advances in phase and moves into a decelerating region of the plasma wakefield. Given fixed laser parameters and acceleration length, dephasing can be mitigated by introducing a density upramp along the accelerating region<sup>18-20</sup>. An increasing plasma density de-

creases the local plasma wavelength. As the electrons travel through the LPA and move closer to the laser pulse, a decreasing plasma wavelength can keep the electron bunch in the accelerating portion of the wake. Density gradients have been shown to increase electron energy in mm-scale gas targets<sup>21,22</sup> at sub-GeV energies. To apply such gradients for LPAs at 10 GeV and beyond would require targets that are 10s of cm long, with density tapering not previously achieved.

In this paper, we experimentally demonstrate that the tapering profiles derived analytically and via simulations can be achieved through simple adjustments to the meter-scale gas jet that was previously used (not tapered) to achieve peak electron energies up to 10 GeV<sup>17</sup>. To support our experimental gas density profile measurements, we simulated gas jet nozzles in OpenFOAM<sup>23</sup> and show good agreement with the experimental measurements. Particle-in-cell (PIC) simulations, performed with the code INF&RNO<sup>24,25</sup>, indicate that using 19 J of laser energy<sup>17</sup>, linear tapering of a 30 cm-long gas jet could result in a  $9\times$  increase in charge and a 32% increase in electron energy compared to the results obtained in the untapered case.

## II. GAS DENSITY MEASUREMENTS

In our experiments, three different gas jets similar in design to Ref. 15, 26–29 were used: (i) a 30 cm long gas jet with 10 equally spaced solenoid valves<sup>17</sup> that fed into an elongated de Laval nozzle with an elliptical cross section<sup>29</sup> (shown in Figure 1d); (ii) a 5 cm long jet that is otherwise identical except that it uses 4 valves; and (iii) a 2 cm jet with 1 solenoid valve and a straight diverging section shown in Figure 1f.

The converging section of the elliptical nozzles have a 2 mm inlet, which linearly converges to a 200  $\mu\text{m}$  throat. Its diverging section consists of elliptical arc walls with a major axis along the center of the nozzle and minor axis at the exit of the nozzle. The straight nozzle has a rectangular inlet section with a length of 4 mm and a width of 3 mm. The diverging section starts from a throat 0.5 mm wide and expands linearly to a width of 3.5 mm.

Our experimental setup is shown in Figure 1a. The gas jet is

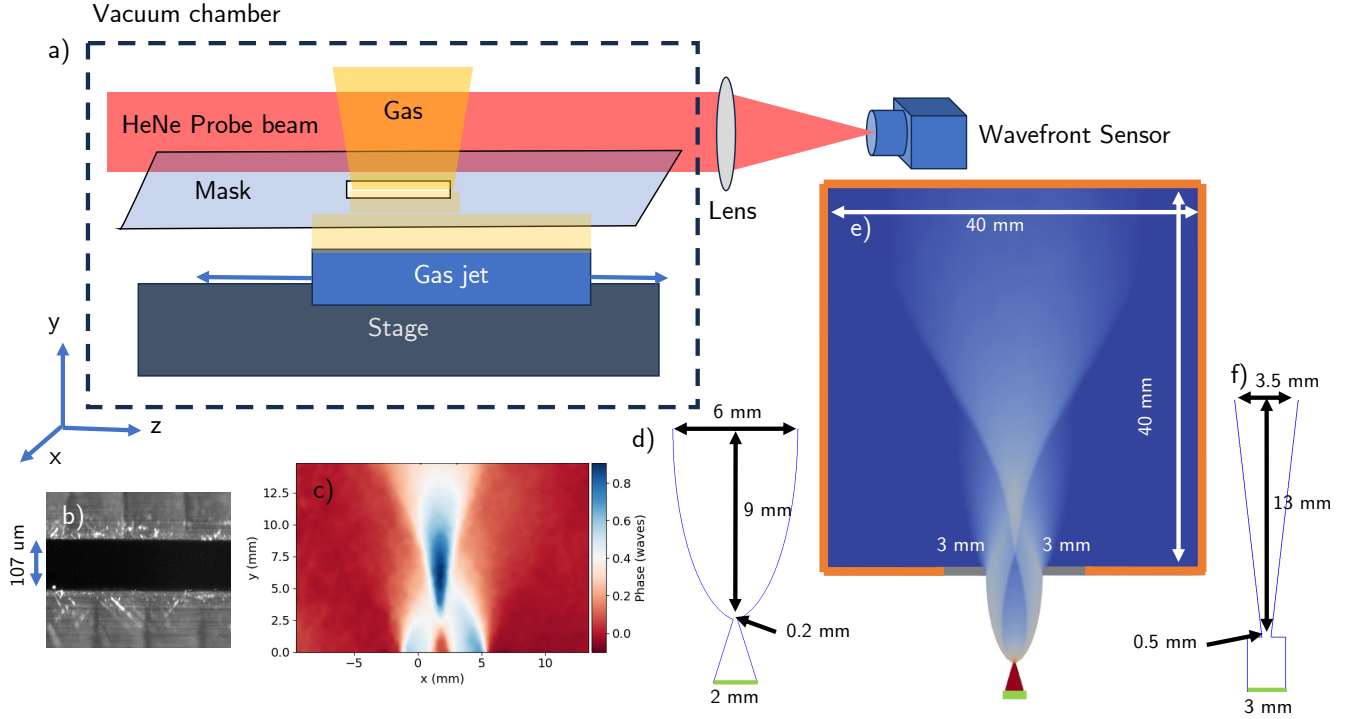


FIG. 1. a) Gas jet density measurement setup. The phase offset of the probe beam ( $\sim 3$  cm diameter) was measured by a wave front sensor after it passes through the gas plume. b) Example microscope image of gas jet throat used for width measurements. c) Raw phase data measured from a representative shot. d) and f) show the elliptical and straight nozzle geometries, respectively. The simulation domain is shown in e), with inlet shown in green, outlet shown in orange, and additional walls near the nozzle in gray.

mounted on a stage that moves longitudinally along the optical axis. An aluminum plate blocked all but a short section of the gas jet, which allowed the longitudinal component of the gas density profile to be measured. The plate contained plastic inserts that diverted gas flow from the masked region of the gas jet towards the ends of the jet to not disrupt the unmasked flow. To verify that the plate did not significantly impact gas flow, we compared the measured gas density of the entire 30 cm gas jet without the plate to the gas jet with the plate. We found no significant differences in the shape of the gas density profile or in the quantitative gas density. A 633 nm HeNe continuous wave (CW) laser was used as a probe beam. A high-resolution wavefront sensor (*Imagine Optic HASO LIFT 680*) was used to measure the phase offset caused by the different index of refraction between gas and vacuum.

To measure the longitudinal density profile of the gas jet, the phase shifts of the probe beam were measured with the gas jet at different positions on the stage. The backing pressure was set to  $1.48 \times 10^6$  Pa. At this pressure, we measured that the valves began to open at  $\sim 3.5$  ms after the initial trigger and reached steady state  $\sim 1$  ms later. We took density data at 4.5 ms after the trigger to ensure that timing fluctuations did not affect the gas density.

We found that ray deflection due to the gradient of index of refraction in the transverse directions was not a significant source of error. The misalignment of the gas jet with respect to the laser, which we estimate to be less than 3.3 mrad, was also an insignificant source of error.

The gas density can be calculated with the formula<sup>30</sup>

$$n(x, y) = \frac{2\epsilon_0 \phi(x, y)\lambda}{\alpha 2\pi L}, \quad (1)$$

where  $n$  is the number density,  $\phi$  is the phase offset in radians,  $\lambda$  is the probe beam wavelength,  $L$  is the length of the hole in the mask,  $\alpha$  is the polarizability of the gas, and  $\epsilon_0$  is the permittivity of free space. We used  $N_2$ , which has an  $\alpha$  of  $19.62 \times 10^{-41}$  F  $\cdot$  m<sup>2</sup> at 633 nm<sup>30</sup>.

### III. SIMULATION METHODS

Gas jet nozzles were simulated in OpenFOAM<sup>23</sup>. Since the exact shape of the nozzle has a large impact on the transverse gas density profile<sup>29</sup>, computational fluid dynamics simulations can allow us to understand the effects of geometry changes on gas density distribution. Nozzles were simulated in 2D due to the lengthwise symmetry of the system. The valves are not simulated because 3D simulations with a complex geometry would be required, greatly increasing the computation resources required. The simulation domain with our gas jet geometries is shown in Figure 1e.

The simulations used hydrogen gas with a Sutherland viscosity model, given by

$$\mu = \frac{A_s T^{1.5}}{T + T_s}, \quad (2)$$

where  $\mu$  is the dynamic viscosity in Pa  $\cdot$  s,  $T$  is temperature in K, and  $A_s$  and  $T_s$  are constants. We used  $A_s = 8.59 \times 10^{-7}$  Pa  $\cdot$

$s K^{-0.5}$  and  $T_s = 273K$  in our simulations. The standard  $k-\varepsilon$  RAS turbulence model<sup>31</sup> with constants from Ref. 32 was used to model turbulence.

Meshes for the simulations were created using Gmsh<sup>33</sup>. A quadrilateral mesh was made using the Frontal-Delaunay method<sup>34</sup>. The mesh sizes are approximately  $r_t/3$  near the throat,  $r_t/1.5$  close to the walls of the nozzle and the inlet,  $200 \mu\text{m}$  in the center of the nozzle and directly to the right of the jet, and 1 mm near the outlet, with an approximately linear mesh size gradient at all other points in the simulation domain.  $r_t$  refers to the throat width of the nozzle. The inlet boundary condition was set to a constant uniform pressure, which was chosen to quantitatively match experimental data. This was necessary because the pressure at the inlet of the nozzle was not known in experiment. Instead, the backing pressure was set at the valves of the gas jet. The outlet boundary condition was an outflow boundary condition with pressure at infinity set to 1 Pa. The initial vacuum pressure was set to 100 Pa for numerical stability. We found no significant differences between simulations with different initial vacuum pressures between 1-1000 Pa.

The solver RhoCentralFoam was used. For each simulation, the mass density was extracted once the simulation reached approximately steady state, which occurs at  $\sim 0.1$  ms. The number density profile was then calculated and compared with experimental results.

#### IV. RESULTS AND DISCUSSION

When using meter-scale gas jets for HOFI experiments, the gas jet must be placed a certain distance, usually  $\gtrsim 5\text{mm}$ , away from the drive beam so that the channel-forming Bessel beam is not blocked by the gas jet. The minimum distance between the drive laser and the jet is lower bounded by the fact that axicon rays will be reflected if their angle is too shallow. For a 30 cm jet, 800 nm laser, and plasma density of  $2 \times 10^{17} \text{cm}^{-3}$ , the minimum angle required is  $\sim 1^\circ$ , which corresponds to  $\sim 5$  mm over the 30 cm jet length. One goal for LPA experiments is to achieve the appropriate gas density with the lowest amount of gas possible because the pump rate of vacuum pumps limits the repetition rate in LPA experiments. Current experiments have been limited to  $< 1$  Hz for this reason. We use the simulated gas density to mass flow rate ratio as a figure of merit for repetition rate; the higher this ratio is, the higher the gas jet repetition rate can be.

The shape of the nozzle has a large impact on the transverse gas density to mass flow rate profile<sup>29</sup>. We measured the gas density profile of an elliptical and straight nozzle in experiment and simulation. The density profiles of the 5 cm elliptical and the 2 cm straight gas jet are shown side by side with their respective simulations in Figure 2. Both density profiles were measured without a mask. The 5 cm elliptical jet was used instead of the 30 cm elliptical jet because when a 30 cm jet is used with a mask, the data  $\leq 4$  mm from the nozzle is distorted due to diffraction from the probe beam off the mask. The 5 cm elliptical jet gives the same measured density distribution as the 30 cm elliptical jet up to a constant factor that is due to differences in the mass flow rate of the valves. The simulated and experimental density profiles of the 2 cm straight jet were normalized such that the simulated mass flow

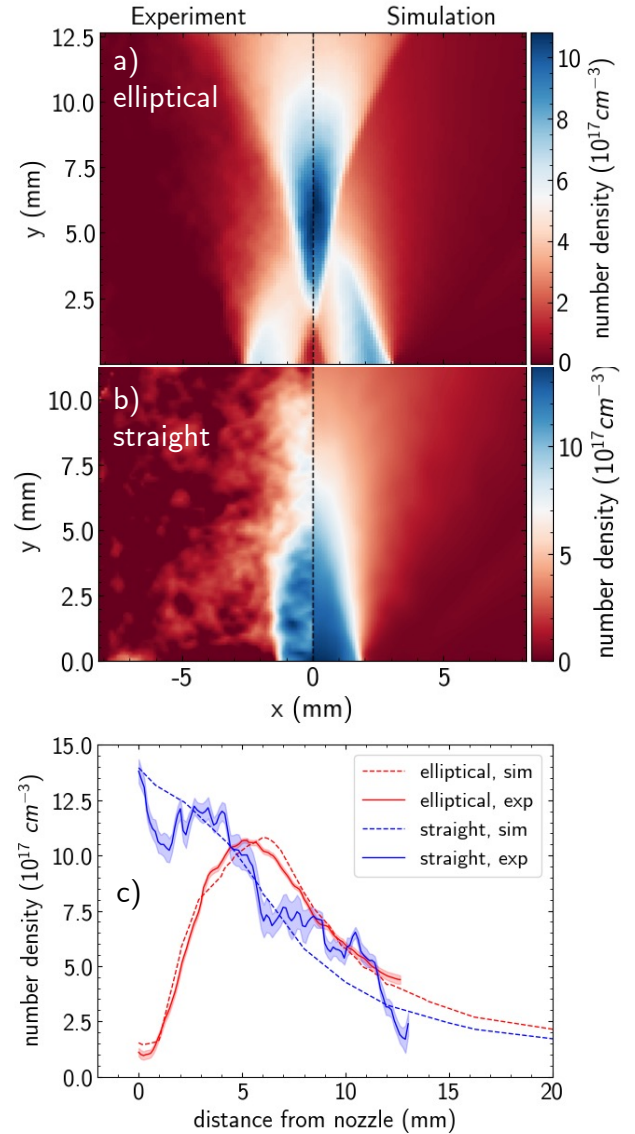


FIG. 2. The experimental and simulated gas density profiles are shown side by side in a) and b), for the elliptical and straight nozzle shape, respectively. Since shot to shot fluctuations in the laser were the dominant source of noise, the lower length of the 2 cm jet results in it having increased noise compared to the 5 cm jet. A lineout at  $x = 0$  is shown for both shapes in c), with experimental measurements in solid lines and simulation results in dashed lines.

rates through the elliptical and straight nozzles were identical. We observe good agreement between experiment and simulation for both the elliptical and straight nozzles.

The shape of the gas density profile for the elliptical nozzle is different than for a straight de Laval nozzle. In a straight de Laval nozzle, the density decreases monotonically with distance from the nozzle since the gas flow diverges. However, in the elliptical nozzle, the gas is focused  $\sim 6$  mm away from the nozzle and then starts to diverge. This caused the molecular density to peak at 6 mm and decrease approximately inversely proportional to the distance from the nozzle exit for heights  $> 6$  mm. The elliptical nozzle shapes gas flow such that the peak density position is optimal for LPA experiments, which enables a 30-40% higher molecular density to mass flow rate

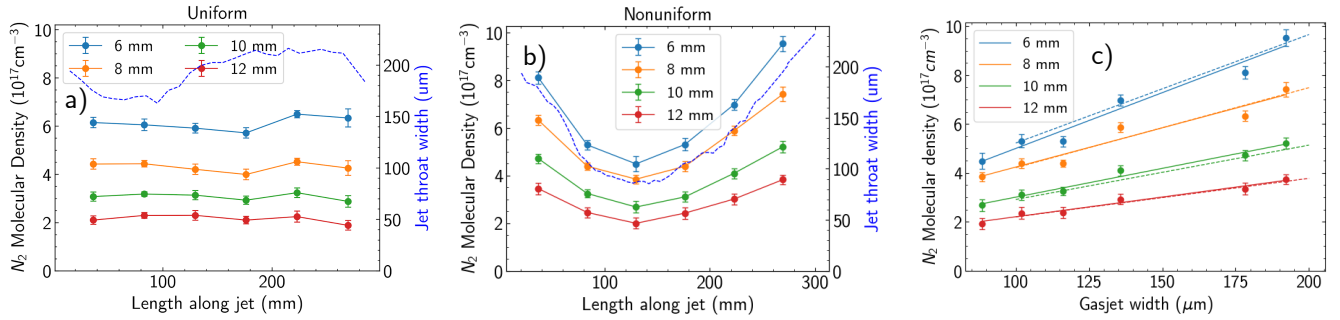


FIG. 3. Measured longitudinal density profile of the uniform throat width and nonuniform throat width configuration are shown in a) and b), respectively. Dashed lines plot nozzle throat width. The linear correlation between nozzle throat width and molecular density is shown in c) for different heights above the nozzle exit. Experimental regressions are shown in solid lines and simulated predictions are shown in dashed lines.

ratio 6-12 mm away from the nozzle compared to a straight jet. This could allow for up to 30-40% higher repetition rate.

Tapering can be achieved by exploiting the density gradient with respect to height. By tilting the gas jet such that the back of the jet is closer to the drive beam, but still  $>6$  mm away, tapering can be achieved in the elliptical jet. The elliptical nozzle also reduces the risk of laser damage since the drive laser will be at least 6 mm below the nozzle.

We controlled the gas jet's longitudinal density profile via throat width adjustments. We tested two different throat width configurations with the elliptical nozzle: a uniform and a nonuniform case. The longitudinal gas density profile at different heights and the throat width profile for both configurations are shown in Figure 3. We find that for the uniform case, the RMS longitudinal density variations are 4-6% between 6 and 12 mm above the nozzle, while the RMS throat width variation is 9.3%. The shot-to-shot density fluctuations can be  $<1\%$ , the measurement being limited by shot-to-shot fluctuations in the probe laser. There is a linear correlation between throat width and molecular density for heights  $>6$  mm above the nozzle exit, which corresponds to the region above the density maximum. This correlation was verified by simulations of nozzles with different throat widths with the same inlet pressure.

The data indicate there are two simple methods for varying the density profile, (i) changing the throat width and (ii) tilting the gas jet. By tilting a constant throat width nozzle, we can achieve a linearly tapered density profile. For more complex density profiles, a combination of tilt and throat width adjustments can be used to generate an arbitrary longitudinal density profile.

The characteristic longitudinal plasma density gradient required to mitigate dephasing can be estimated with an analytical 1-D model (see, e.g., Ref.<sup>20</sup>). We have,

$$\frac{n(z)}{n_0} \approx 1 + \frac{\pi}{|\Psi_0|} \frac{z}{L_d}, \quad L_d = \pi \frac{k_0^2}{k_{p0}^3}, \quad (3)$$

where  $n(z)$  is the plasma density,  $n_0 = n(z=0)$  is the plasma density at the upstream end of the jet,  $|\Psi_0|$  is the phase of the electrons behind the laser driver,  $L_d$  is the dephasing length,  $k_0$  is the laser wavenumber, and  $k_{p0}$  is the plasma wavenumber at the upstream end of the jet. For an electron bunch loaded in the first plasma period  $|\Psi_0| \sim 2\pi$ , and so the expected plasma

density increase over a dephasing length is  $n(z=L_d)/n_0 \sim 2$ . Density profiles corresponding to this gradient can be experimentally realized by tilting the uniform configuration jet by 11 mrad, and positioning the upstream end of the jet 12 mm below the drive laser as shown in Fig. 4.

We numerically investigated, by means of PIC simulations performed with the code INF&RNO<sup>24,25</sup>, the role of tapering in the performance of a 30 cm-long, 10 GeV-class LPA with the laser and plasma parameters discussed in Ref. 17. The improvement of LPA performance obtainable by tapering the longitudinal plasma density profile is shown in Fig. 4(a), where we compare the electron beam spectrum produced and accelerated in an LPA with uniform longitudinal density (black spectrum) to that obtained in the case of tapered density (red spectrum), where the final density is 2.5 times higher than at the entrance. In both cases the LPA is driven by a laser pulse with an energy of 19 J, a pulse duration of 40 fs (FWHM of the intensity), and a  $53 \mu\text{m}$  laser spot. The laser mode and the initial transverse density profile are the ones described in Figure 1(c) of Ref. 17. Note that the channel depth is kept constant along the channel length in these simulations. We expect this to be a good approximation as, in the HOFI channel generation, the radial position of the hydrodynamic shock front is approximately independent of density. This can be understood from Sedov-Taylor theory<sup>35</sup>, since the shock front radius is  $r_s \propto (\mathcal{E}/n_0)^{1/4}$ , where  $\mathcal{E}$  is the energy deposited per unit length, and  $\mathcal{E} \propto n_0$  for energy deposition using optical field ionization. The value of the on-axis density at the entrance of the plasma is  $1.05 \times 10^{17} \text{ cm}^{-3}$ . Electron beams were generated by introducing a nitrogen dopant (1% nitrogen / 99% hydrogen) in the gas jet, enabling ionization-induced injection. In the constant density case the dopant is restricted in the first 12 cm of the plasma. In the tapered case the dopant is restricted in the region 8-10 cm. In the uniform density case beams with a charge of 9 pC and an average energy of 9.4 GeV after 30 cm of propagation in plasma are produced. By tapering the longitudinal density profile, the charge increases to 81 pC and the energy to 12.4 GeV. The longitudinally uniform jet tilted at 14 mrad and positioned such that the upstream end of the jet is 12 mm below the drive laser (see Figure 4) was able to replicate this density taper.

For both the analytical and simulated tapering profile, the densities are normalized such that at  $z=0$ ,  $n/n_0 = 1$  because the molecular density can be arbitrarily scaled by changing

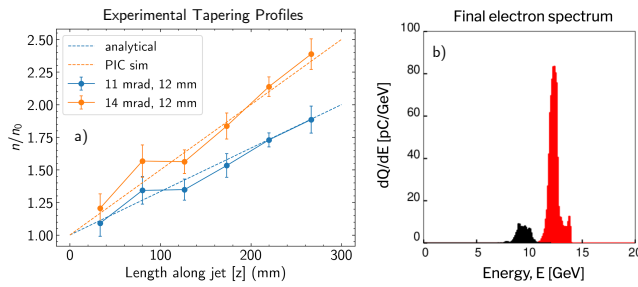


FIG. 4. a) The measured, normalized gas densities of the longitudinally uniform gas jet at different heights and different gas jet tilts are shown in circles with solid lines, highlighting linear tapering over 30 cm. The analytically calculated and simulated tapering profiles are shown in dashed lines. b) The simulated electron spectrum with and without tapering is shown in red and black, respectively.

the backing pressure or the number of valves on the jet.

## V. CONCLUSION

Longitudinal density profiles appropriate for tapering were created using a meter-scale gas jet. We showed that by adjusting two simple parameters, the angle of the jet and the throat width, arbitrary slowly-varying density distributions could be generated. An experimental platform was constructed to measure the 3-D density distribution of meter-scale gas jets. An elliptical nozzle shape was experimentally measured and simulated, and was shown to have a higher peak density to mass flow rate ratio than a straight de Laval nozzle. Tapered density profiles relevant to the BELLA laser system were simulated and experimentally matched using a tilted 30 cm gas jet, proving through simulations that  $>10$ -GeV scale tapering is in reach for future experiments with laser drivers as low as 19 Joule.

## ACKNOWLEDGMENTS

This work was supported by the Defense Advanced Research Projects Agency, the Director, Office of Science, Office of High Energy Physics, of the U.S. Department of Energy under Contract No. DE-AC0205CH11231, and used the computational facilities at the National Energy Research Scientific Computing Center (NERSC). The authors thank Teo Maldonado Mancuso, Zac Eisentraut, Mark Kirkpatrick, Federico Mazzini, Nathan Ybarrolaza, Derrick McGrew, and Chetanya Jain for technical support.

## AUTHOR DECLARATIONS

### Conflicts of Interest

The authors have no conflicts to disclose.

## Author Contributions

**R. Li:** Conceptualization (equal), Data curation (lead), Formal analysis (lead), Methodology (lead), Investigation (lead), Visualization (lead), Writing - original draft (lead). **A. Picksley:** Conceptualization (equal), Data curation (equal), Formal analysis (equal), Methodology (equal), Visualization (equal), Writing - review and editing (equal). **C. Benedetti:** Data curation (equal), Formal analysis (equal), Writing - original draft (equal), Writing - review and editing (equal). **F. Filippi:** Data curation (equal), Formal analysis (equal), Writing - review and editing (equal). **J. Stackhouse:** Formal analysis (equal), Methodology (equal). **L. Fan-Chiang:** Data curation (equal), Methodology (equal). **H. E. Tsai:** Formal analysis (equal), Methodology (equal). **K. Nakamura:** Project administration (equal), Supervision (equal). **C. B. Schroeder:** Project administration (equal), Funding acquisition (lead), Supervision (equal), Writing - review and editing (equal). **J. van Tilborg:** Project administration (equal), Funding acquisition (equal), Writing - review and editing (equal). **E. Esarey:** Project administration (equal), Funding acquisition (equal). **C. G. R. Geddes:** Project administration (equal), Funding acquisition (equal). **A. J. Gonsalves:** Conceptualization (lead), Writing - review and editing (equal), Project administration (equal), Funding acquisition (equal), Supervision (lead).

## DATA AVAILABILITY STATEMENT

The data that support the findings of this study are available from the corresponding author upon reasonable request.

- <sup>1</sup>T. Tajima and J. M. Dawson, Phys. Rev. Lett. **43**, 267 (1979).
- <sup>2</sup>E. Esarey, C. B. Schroeder, and W. P. Leemans, Reviews of modern physics **81**, 1229 (2009).
- <sup>3</sup>W. Wang, K. Feng, L. Ke, C. Yu, Y. Xu, R. Qi, Y. Chen, Z. Qin, Z. Zhang, M. Fang, *et al.*, Nature **595**, 516 (2021).
- <sup>4</sup>C. B. Schroeder, E. Esarey, C. Geddes, C. Benedetti, and W. P. Leemans, Physical Review Special Topics—Accelerators and Beams **13**, 101301 (2010).
- <sup>5</sup>C. G. Geddes, S. Rykovanov, N. H. Matlis, S. Steinke, J.-L. Vay, E. H. Esarey, B. Ludewigt, K. Nakamura, B. J. Quiter, C. B. Schroeder, *et al.*, Nuclear Instruments and Methods in Physics Research Section B: Beam Interactions with Materials and Atoms **350**, 116 (2015).
- <sup>6</sup>A. Borisov, A. Borovskiy, V. Korobkin, A. Prokhorov, O. Shiryaev, X. Shi, T. Luk, A. McPherson, J. Solem, K. Boyer, *et al.*, Physical review letters **68**, 2309 (1992).
- <sup>7</sup>K. Krushelnick, A. Ting, C. Moore, H. Burrell, E. Esarey, P. Sprangle, and M. Baine, Physical review letters **78**, 4047 (1997).
- <sup>8</sup>C. Durfee III and H. Milchberg, Physical review letters **71**, 2409 (1993).
- <sup>9</sup>A. Zigler, Y. Ehrlich, C. Cohen, J. Krall, and P. Sprangle, JOSA B **13**, 68 (1996).
- <sup>10</sup>A. Butler, D. Spence, and S. M. Hooker, Physical Review Letters **89**, 185003 (2002).
- <sup>11</sup>R. J. Shalloo, C. Arran, L. Corner, J. Holloway, J. Jonnerby, R. Walczak, H. Milchberg, and S. M. Hooker, Physical Review E **97**, 053203 (2018).
- <sup>12</sup>R. Shalloo, C. Arran, A. Picksley, A. Von Boetticher, L. Corner, J. Holloway, G. Hine, J. Jonnerby, H. Milchberg, C. Thornton, *et al.*, Physical Review Accelerators and Beams **22**, 041302 (2019).
- <sup>13</sup>A. Picksley, A. Alejo, R. Shalloo, C. Arran, A. Von Boetticher, L. Corner, J. Holloway, J. Jonnerby, O. Jakobsson, C. Thornton, *et al.*, Physical Review E **102**, 053201 (2020).
- <sup>14</sup>L. Feder, B. Miao, J. Shrock, A. Goffin, and H. Milchberg, Physical Review Research **2**, 043173 (2020).
- <sup>15</sup>B. Miao, J. E. Shrock, L. Feder, R. C. Hollinger, J. Morrison, R. Nedbailo, A. Picksley, H. Song, S. Wang, J. J. Rocca, and H. M. Milchberg, Phys. Rev. X **12**, 031038 (2022).

- <sup>16</sup>J. Shrock, B. Miao, L. Feder, and H. Milchberg, *Physics of Plasmas* **29** (2022).
- <sup>17</sup>A. Picksley, J. Stackhouse, C. Benedetti, K. Nakamura, H. E. Tsai, R. Li, B. Miao, J. E. Shrock, E. Rockafellow, H. M. Milchberg, C. B. Schroeder, J. van Tilborg, E. Esarey, C. G. R. Geddes, and A. J. Gonsalves, “Matched guiding and controlled injection in dark-current-free, 10-gev-class, channel-guided laser plasma accelerators,” (2024), arXiv:2408.00740 [physics.plasm-ph].
- <sup>18</sup>H. Suk, C. Kim, G. Kim, J. Kim, I. Ko, and H. Lee, *Physics Letters A* **316**, 233 (2003).
- <sup>19</sup>A. Pukhov and I. Kostyukov, *Physical Review E—Statistical, Nonlinear, and Soft Matter Physics* **77**, 025401 (2008).
- <sup>20</sup>W. Rittershofer, C. B. Schroeder, E. Esarey, F. J. Grüner, and W. P. Leemans, *Physics of Plasmas* **17**, 063104 (2010).
- <sup>21</sup>E. Guillaume, A. Döpp, C. Thaury, K. Ta Phuoc, A. Lifschitz, G. Grittani, J.-P. Goddet, A. Tafzi, S. W. Chou, L. Veisz, and V. Malka, *Phys. Rev. Lett.* **115**, 155002 (2015).
- <sup>22</sup>C. Aniculaesei, V. B. Pathak, H. T. Kim, K. H. Oh, B. J. Yoo, E. Brunetti, Y. H. Jang, C. I. Hojota, J. H. Shin, J. H. Jeon, *et al.*, *Scientific Reports* **9**, 11249 (2019).
- <sup>23</sup>H. Jasak, A. Jemcov, Z. Tukovic, *et al.*, in *International workshop on coupled methods in numerical dynamics*, Vol. 1000 (Dubrovnik, Croatia), 2007) pp. 1–20.
- <sup>24</sup>C. Benedetti, C. Schroeder, E. Esarey, and W. Leemans, in *AIP Conference Proceedings*, Vol. 1507 (American Institute of Physics, 2012) pp. 252–257.
- <sup>25</sup>C. Benedetti, C. Schroeder, C. Geddes, E. Esarey, and W. Leemans, *Plasma Physics and Controlled Fusion* **60**, 014002 (2017).
- <sup>26</sup>M. KRISHNAN, “Linear gas jet with tailored density profile,” Tech. Rep. (Alameda Applied Sciences Corporation, 2012).
- <sup>27</sup>M. Krishnan, “A novel gas jet for laser wakefield acceleration,” Tech. Rep. (Alameda Applied Sciences Corporation, 2012).
- <sup>28</sup>D. E. Mittelberger, M. Thévenet, K. Nakamura, A. J. Gonsalves, C. Benedetti, J. Daniels, S. Steinke, R. Lehe, J.-L. Vay, C. B. Schroeder, *et al.*, *Physical Review E* **100**, 063208 (2019).
- <sup>29</sup>O. Zhou, H.-E. Tsai, T. M. Ostermayr, L. Fan-Chiang, J. Van Tilborg, C. B. Schroeder, E. Esarey, and C. G. Geddes, *Physics of Plasmas* **28** (2021).
- <sup>30</sup>J. P. Couperus, A. Köhler, T. Wolterink, A. Jochmann, O. Zarini, H. Bastiaens, K. Boller, A. Irman, and U. Schramm, *Nuclear Instruments and Methods in Physics Research Section A: Accelerators, Spectrometers, Detectors and Associated Equipment* **830**, 504 (2016).
- <sup>31</sup>B. E. Launder and B. I. Sharma, *Letters in heat and mass transfer* **1**, 131 (1974).
- <sup>32</sup>S. H. El-Tahry, *J. Energy;(United States)* **7** (1983).
- <sup>33</sup>C. Geuzaine and J.-F. Remacle, *International Journal for Numerical Methods in Engineering* **79** (2009).
- <sup>34</sup>S. Rebay, *Journal of computational physics* **106**, 125 (1993).
- <sup>35</sup>R. J. Shalloo, C. Arran, L. Corner, J. Holloway, J. Jonnerby, R. Walczak, H. M. Milchberg, and S. M. Hooker, *Phys. Rev. E* **97**, 053203 (2018).